Combustion and Flame 213 (2020) 226–236

Contents lists available at ScienceDirect

Combustion and Flame

journal homepage: www.elsevier.com/locate/combustflame

Ignition delay time measurement and kinetic modeling of furan, and comparative studies of 2,3-dihydrofuran and tetrahydrofuran at low to intermediate temperatures by using a rapid compression machine

Yingtao Wu[a], Nan Xu[b], Meng Yang[a], Yang Liu[a], Chenglong Tang[a,*], Zuohua Huang[a]

[a] State Key Laboratory of Multiphase Flow in Power Engineering, Xi'an Jiaotong University, Xi'an 710049, China
[b] GAC Automotive Research & Development Center, No. 668 Jinshan Road East, Panyu District, Guangzhou, Guangdong, China

ARTICLE INFO

Article history:
Received 27 September 2019
Revised 3 December 2019
Accepted 4 December 2019
Available online 20 December 2019

Keywords:
Rapid compression machine (RCM)
Ignition delay time
Furan
2,3-dihydrofuran
Tetrahydrofuran

ABSTRACT

The low to intermediate temperature (850–1050 K) auto-ignition characteristics of furan, 2,3-dihydrofurn and tetrahydrofuran have been investigated both experimentally and kinetically. The pressure (18 and 33 bar) and equivalence ratio (0.5, 1.0 and 2.0) effects on the auto-ignition of furan were experimentally examined using a rapid compression machine. Compared with alkylated furans, the ignition delay times of furan show notably insensitivity to equivalence ratio. Comparison on the low to intermediate temperature reactivity of furan, alkylated furans, 2, 3-dihydrofuran, and tetrahydrofuran indicates that saturation degree plays a more dominant role in enhancing reactivity than alkyl substitution. Literature mechanisms were validated against present data. Kinetic analyses revealed the major fuel consuming routes and the causes for the deviation between simulation and experimental results. Furthermore, a modified model of furan, 2, 3-dihydrofuran, and tetrahydrofuran was proposed and validated against the ignition delay times in this study as well as experimental data in literatures.

1. Introduction

Biofuels are treated as promising alternatives to the depletion of traditional fossil fuels. Without putting a threat on food safety, the furanic fuels can be produced from lignocellulosics [1–3]. Improved production methods of furanic fuels make them as possible fossil fuel alternatives. The furanic fuels mainly comprise of alkylfurans, dihydrofurans, and tetrahydrofurans. Furan, a ring structured and unsaturated ether, is the simplest component of furanic fuels and it can be produced from the pyrolysis of leaves, wood and tobacco smoke [4]. Furan is also an important intermediate during the oxidation of other alkylfuran components [5,6], including 2, 5-dimethylfuran (DMF25), 2-methylfuran (MF2), and 2-ethylfuran (EF2).

Relative to the degree of study conducted on DMF25 and MF2, furan has seen less exploratory analysis [7]. Tian et al. [8] examined the profiles of more than 40 species for low pressure premixed furan flames and constructed the furan mechanism. Wei et al. [9] have measured the high temperature ignition delay times (IDTs) of furan at pressures up to 10.4 atm and some attempts have been made for mechanism optimization. Other researchers aimed to conduct comparative studies on the combustion kinetics of furan. Liu et al. [10], Tran et al. [11], and Togbe et al. [12] conducted a series of research towards the detailed flame structures of furan, MF2, and DMF25 respectively. A single kinetic mechanism was constructed for the modeling of the three fuels. The furan sub-mechanism was refined, showing better agreement with their experimental results. They concluded that the structure differences would induce varied species profiles of CO, C_2H_2, C_2H_6, and 1, 3-C_4H_6. Eldeeb and Akih-Kumgeh [13] compared the high temperature IDTs of furan, MF2, and DMF25 under air-dilution conditions, finding that the reactivity of MF2 is the highest, followed by furan and then DMF25. Xu et al. [14] studied the ignition characteristics of DMF25, MF2, and furan in the high temperature range at a constant fuel load, showing that furan is the least reactive. Sudholt et al. [15,16] firstly determined the DCNs (derived cetane number) of alkylfurans and tetrahydrofurans. From their results, the DCNs of tetrahydrofurans are systematically higher than those of furans and the ignition characteristics of furans largely differ from those of tetrahydrofurans. The reactivity of furans is determined by the ring structure, making them suitable SI engine candidates, while that of tetrahydrofurans depends on the side chain properties. Later on, the authors measured the low temperature air-diluted IDTs of alkylfurans and tetrahydrofurans at 20 bar,

* Corresponding author.
E-mail address: chenglongtang@mail.xjtu.edu.cn (C. Tang).

https://doi.org/10.1016/j.combustflame.2019.12.010
0010-2180/

Table 1
Experimental condition.

Fuel	Fuel concentration	P /bar	ϕ
furan	1%	18, 33	0.5, 1.0, 2.0
2,3-DHF	1%	18	1.0
THF	1%	18	1.0

650–900 K, and $\phi = 1.0$. Distinct from furans that longer side chain induces higher low to intermediate temperature reactivity, the reactivity order of tetrahydrofurans is influenced both by the length and the position of the side alkyl chain. Tran et al. [5] measured the stable and intermediate species in the low to intermediate temperature oxidation of furan, MF2, and DMF25 in a flow reactor. They extended the mechanism of Liu et al. [10] for the application in the low to intermediate temperature range, which is in line with experimental results. Most of the above-mentioned researches focus on high temperature regime, and efforts toward low to intermediate ignition characteristics of furan are not sufficiently studied both experimentally and kinetically.

Tetrahydrofuran (THF) is a saturated cyclic ether and a promising candidate for using as engine fuel [17]. Dihydrofuran (DHF) has a very similar molecular structure with furan and THF with one carbon-carbon double bond. Many works [17,18] have contributed to the understanding of THF combustion chemistry. Recently, Fenard et al. [18] have developed a detailed kinetic model of THF including the low-temperature chemistry and it has been validated against the IDTs in both high and low temperature as well as species profiles in a jet-stirred reactor (JSR). However, there are only few studies on the IDTs of dihydrofurans. Fan et al. [19,20] have measured the IDTs of 2,3-dihydrofuran (2,3-DHF) and 2,5-dihydrofuran (2,5-DHF) in the high temperature region using a shock tube and compared the reactivity among furan, 2,3-DHF and 2,5-DHF. To the best of the authors' knowledge, there is no low temperature ignition delay data for 2,3-DHF available in literatures.

This paper firstly provides IDTs of furan, 2,3-DHF and THF in the low to intermediate temperature range, which will be important for the mechanism development. Secondly, literature mechanisms about furans [10,18,21,22] have been validated against present data. Kinetic analyses have been conducted to reveal the major pathways of furan consumption and dominant reactions. Furthermore, the low to intermediate temperature reactivity of alkylfurans, furan, 2,3-DHF and THF are compared to show the effect of alky side chains and unsaturated double bond on the cyclic ether molecular oxidation.

2. Methodology

The IDTs were measured using two rapid compression machines (RCMs) in Xi'an Jiaotong University (XJTU-RCM) and Tsinghua University (TU-RCM) under the same conditions. Details of the facilities can be found in Refs. [23-26], and here only the RCM in Xi'an Jiaotong University is briefly introduced. Five components comprise the apparatus: the high-pressure stainless air tank, the driving section, the hydraulic chamber, the driven section and the reaction vessel. A creviced piston is adopted to prevent the mixing of boundary layer gas with core region due to the roll up vortex. Details of the creviced piston design can be found in Ref. [24]. Before the experiments, mixtures are prepared in a vessel according to their partial pressures. Specifically, the partial pressures of the fuels are kept at 1/3 of their saturated vapor pressures. The purities of furan, 2,3-DHF, and THF are 99.5%, 98%, and 99.5% respectively. Experiments were conducted at least an hour later to ensure the homogeneity of the mixtures. Experimental condition is given in Table 1. Mixtures composition and detailed measured IDTs are provided in the Supplementary materials.

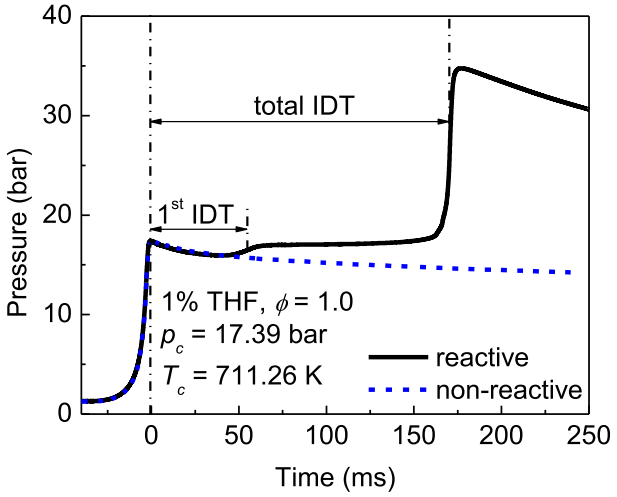

Fig. 1. Typical pressure traces measured in this RCM. Solid line: reactive pressure trace; dash line: non-reactive pressure trace.

Typical measured pressure traces in this RCM are shown Fig. 1. IDT is defined as the time interval between the end-of-compression and the maximum slope $(dp/dt)_{max}$ on the pressure trace. For each reactive compression, a non-reactive case was conducted in which O_2 in the fuel mixture is substituted by the same moles of N_2. Volume profiles [27] were adopted in the simulations to account for the facility effects, which are deduced from non-reactive pressure traces by applying adiabatic compression and expansion theory. The alkylfuran mechanism of Somers et al. [21,22], Liu et al. [10], Tran et al. [5] and THF mechanism of Fenard et al. [18] are used in simulating the auto-ignition at the experimental conditions using Chemkin Pro [28] software.

3. Results and discussion

3.1. The ignition delay times of furan

The IDTs of furan in low to intermediate temperature range (850–1050 K) were measured in two RCMs to confirm the reliability of the experimental data. The maximum measurement discrepancy is within 38% between these two RCM which is ascribed to the measurement uncertainty and facility effect. Detail comparisons on the IDTs obtained from these two apparatuses are provided in the supplementary material. If not specified, IDTs discussed in the following sections were measured in XJTU-RCM. Figure 2 depicts the influence of equivalence ratio and pressure on the IDTs of furan. The IDTs of furan increase linearly with reciprocal temperature, and no NTC (negative temperature coefficient) or two-stage ignition phenomenon were observed for furan. Due to the cyclic unsaturated structure, it is reasonable that the reactivity of furan is quite limited, and the present IDTs (1% fuel concentration) mainly fall in the intermediate temperature range (900–1010 K). Compared with DMF25, EF2, and MF2 [6,29], the IDTs of furan are not sensitive to the variation of equivalence ratio under constant fuel load of 1%, and increasing only slightly with increasing equivalence ratio (dilution ratio is also changed), as shown in Fig. 2(a). This is consistent with the conversion rate of furan under low to intermediate temperature oxidation conditions [5]. The pressure effect on the IDTs of furan is shown in Fig. 2(b), which clearly indicates the enhancement of reactivity at higher pressures.

3.2. The ignition delay times of 2,3-DHF and THF

The IDTs of stoichiometric mixtures of 2,3-DHF and THF were measured at the pressure of 18 bar, as shown in Fig. 3(a) and (b).

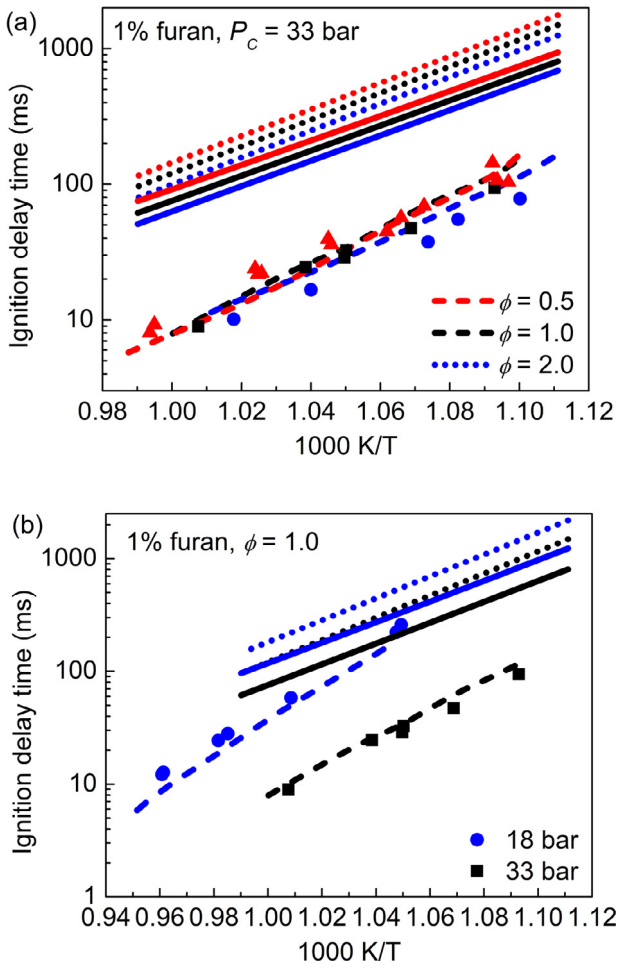

Fig. 2. The influence of equivalence ratio (0.5, 1.0 and 2.0) and pressure (18 and 33 bar) on IDTs of furan under 1% fuel concentration. Solid line: the mechanism of Somers et al. [21,22]; dash line: the mechanism of Tran et al. [5]; dot line: the mechanism of Liu et al. [10]. (For interpretation of the references to color in this figure, the reader is referred to the web version of this article).

The IDTs of 2,3-DHF become shorter as temperature increased, and no two-stage ignition was observed. The ignition of THF, however, exhibits a typical low-temperature reactivity with two-stage behavior, as observed in the pressure trace in Fig. 1. Both the first-stage (1st IDT) and total IDTs are then reported in this work.

3.3. The performance of literature models

3.3.1. Furan sub-models

Being as the fundamental part of furan derivatives, the sub-mechanism of furan is included in the mechanism of alkylfurans and tetrahydrofurans. The NUIG alkylfuran mechanism developed by Somers et al. [21,22] has been validated against pyrolysis, jet stirred reactor species profiles, laminar burning velocities and IDTs of MF2 and DMF25. The mechanism of Liu and co-workers [10-12] has been validated against the oxidation flame structures of furan, MF2, and DMF25. The furan sub-mechanism of these two mechanisms are both from Tian et al. [8], maintaining only minor differences. Recently Tran et al. [5] further extended Liu's model to the low to intermediate temperature range, with new features included in the furan sub-mechanism. However, the performance of these mechanisms against low to intermediate temperature IDTs of furan has not been tested.

In Fig. 2, the simulating results from Somers et al. [21,22], Tran et al. [5], and Liu et al. [10] are depicted with solid, dash, and dot lines respectively. Under the present experimental range, the equivalence ratio effect on the IDTs of furan can be qualitatively captured by the mechanisms of Liu et al. [10] and Somers et al. [21,22], however over-predicted by one magnitude. The mechanism of Tran et al. [5] provides better quantitative agreement with experimental data. However, the mechanism cannot depict the dependent of IDTs on equivalence ratio: at intermediate temperatures (1000 K), IDTs for three equivalence ratios agree with each other, while at lower temperatures, IDTs of ϕ = 2.0 are very close to that of ϕ = 1.0 and higher than that of ϕ = 0.5. In addition, the mechanism of Tran et al. [5] exhibits weaker equivalence ratio dependence compared with experimental results. Although experimentally measured furan ignition delays are quite close under different equivalence ratios, the trend that increasing the equivalence ratio prolongs IDTs under constant fuel loads can still

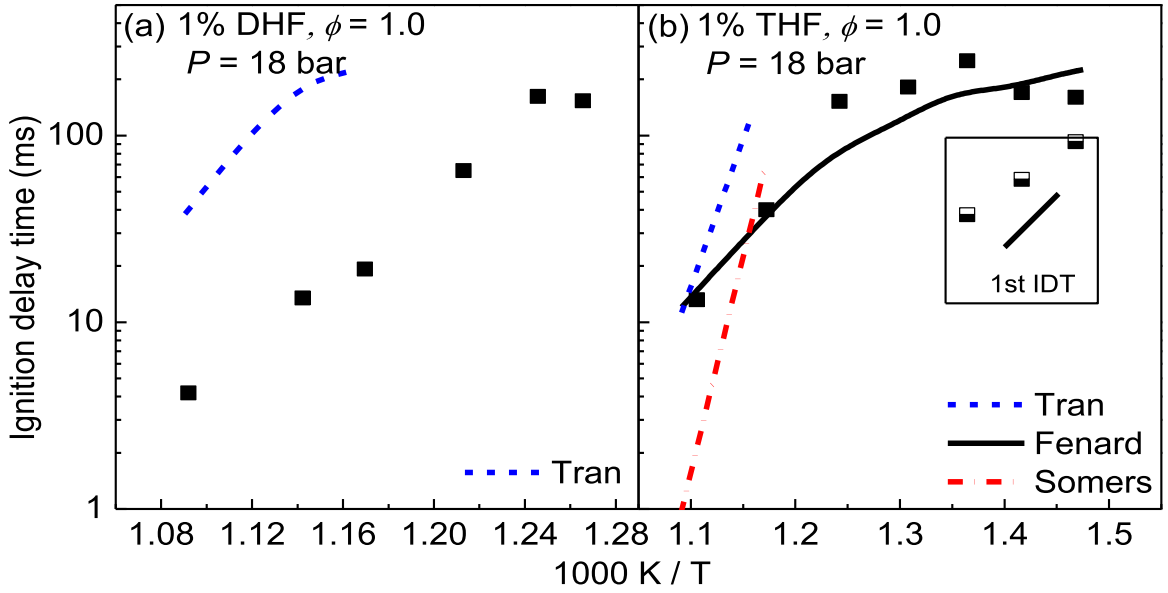

Fig. 3. The IDTs of 2,3-DHF (a) and THF (b) under 1% fuel concentration. Solid line: the mechanism of Fenard et al. [18]; dash dot line: the mechanism of Somers et al. [21,22]; dash lines: the mechanism of Tran et al. [5].

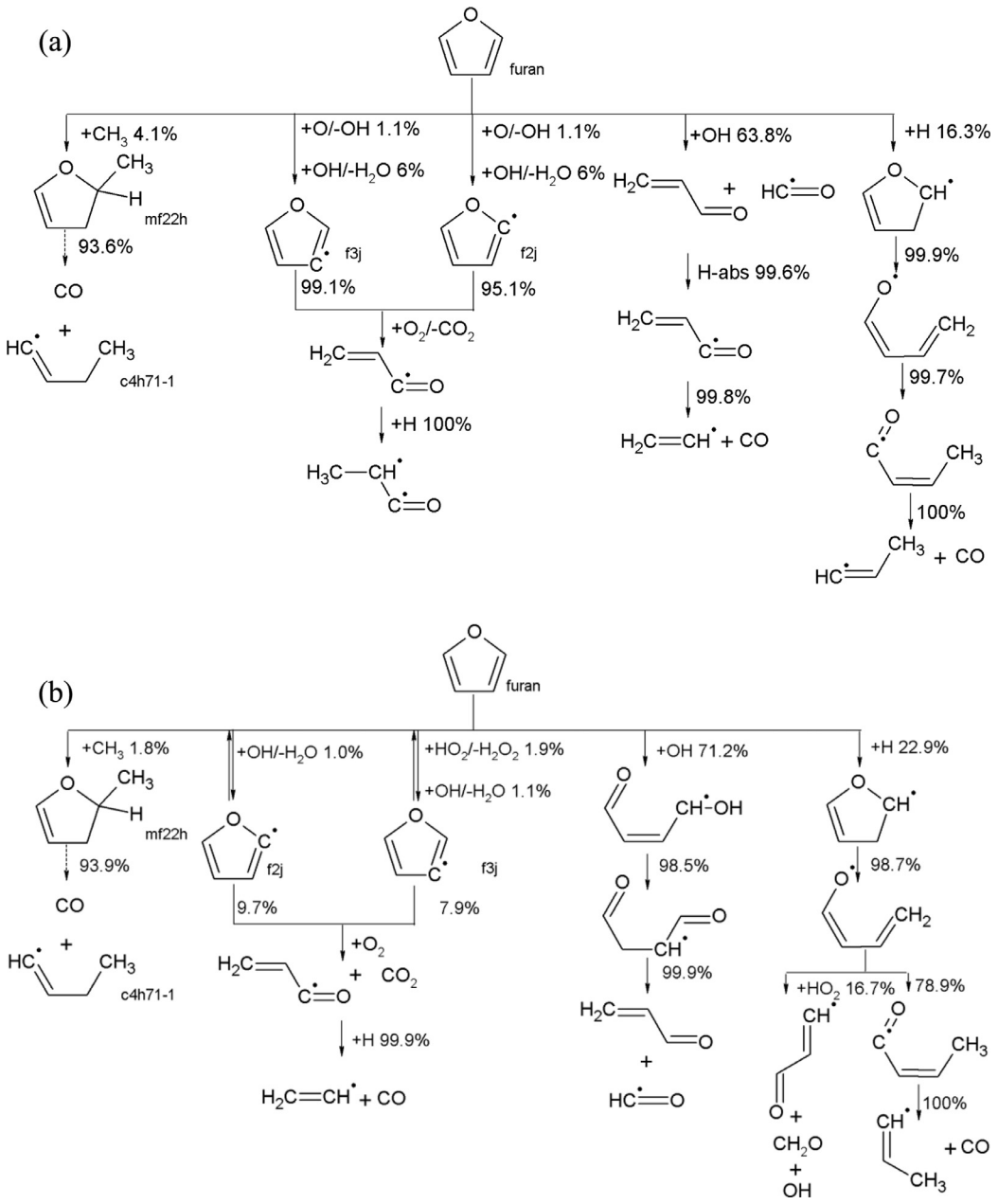

Fig. 4. Reaction pathway analyses of furan at ϕ = 1.0, 900 K, 18 bar and 20% fuel consumption: (a) the mechanism of Somers et al. [21]; (b) the mechanism of Tran et al. [5].

be seen from Fig. 2(a), even with uncertainties taken into account. In the low to intermediate temperature oxidation experiments of furan [5], the conversion rates of furan under different equivalence ratio are quite close and fall in the order: 1.0 > 0.5 > 2.0 both from experiments and simulation of Tran's mechanism. Tran's mechanism also predicts well the IDTs of furan under different pressures, as shown by Fig. 2(b), with only slightly lower predicted IDTs for 18 bar condition.

3.3.2. 2,3-DHF and THF sub-models

The kinetic models of 2,3-DHF and THF are included as sub models in both mechanisms of Tran et al. [5] and Somers et al. [21,22]. Fenard et al. [18] has recently extended the mechanism of THF to low temperature range and also included the sub model of 2,3-DHF. Thus, performance of these three mechanisms is tested against present ignition delay data of 2,3-DHF and THF, as shown in Fig. 3(a) and (b). Since none of these mechanisms has explicitly developed the sub model of 2,3-DHF, all the mechanisms have greatly under-predicted the reactivity of 2,3-DHF in the studied temperature range (780–920 K), and no ignition was predicted by mechanisms of Fenard et al. [18] and Somers et al. [21,22] within 500 ms. In Fig. 3(b), mechanism of Fenard et al. [18] has well captured the IDTs of THF and the mild NTC trend. It should be noted that, this mechanism has also been validated against the RCM data (fuel in air condition) of Vanhove et al. [30] and gives the similar performance. Although this mechanism still needs to be improved for the prediction of NTC and 1st IDT, it generally performs good in both fuel in air and more diluted conditions. Due to the lack of low-temperature reactions, mechanisms of Tran and Somers cannot predict well the ignition at temperatures lower 850 K. In higher temperature region, prediction of Tran model is very close to that of Fenard, while the simulation results of Somers mechanism are more than one magnitude shorter than experimental measurements.

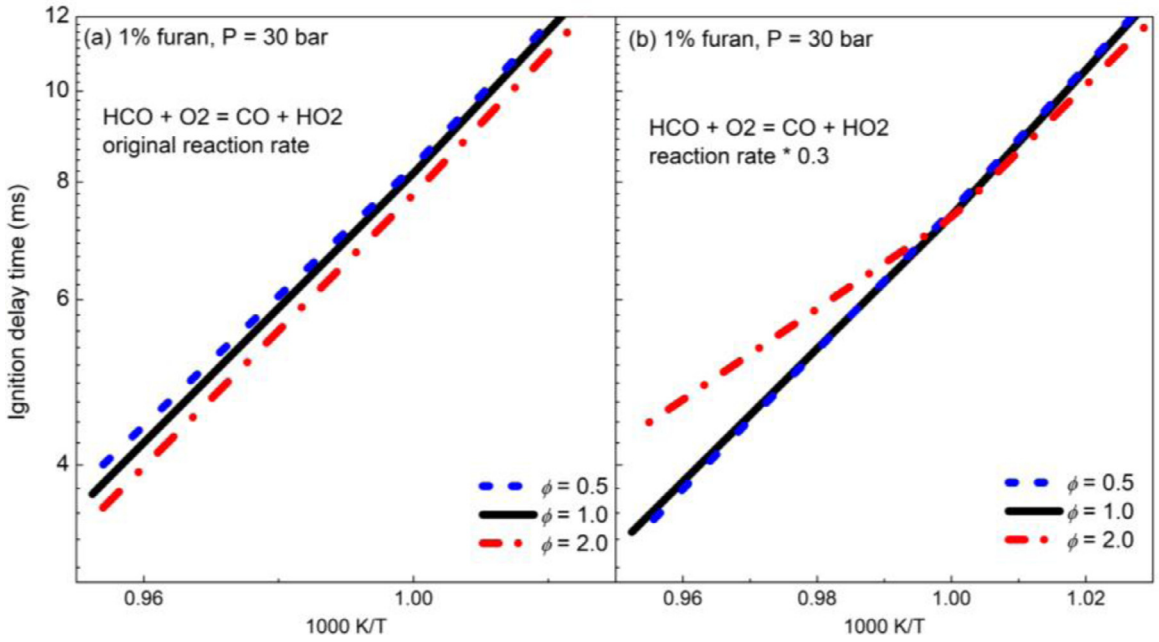

Fig. 5. The influence of the rate constant of reaction HCO + O_2 = CO + HO_2 in Tran mechanism [5] on the low to intermediate temperature IDTs of furan.

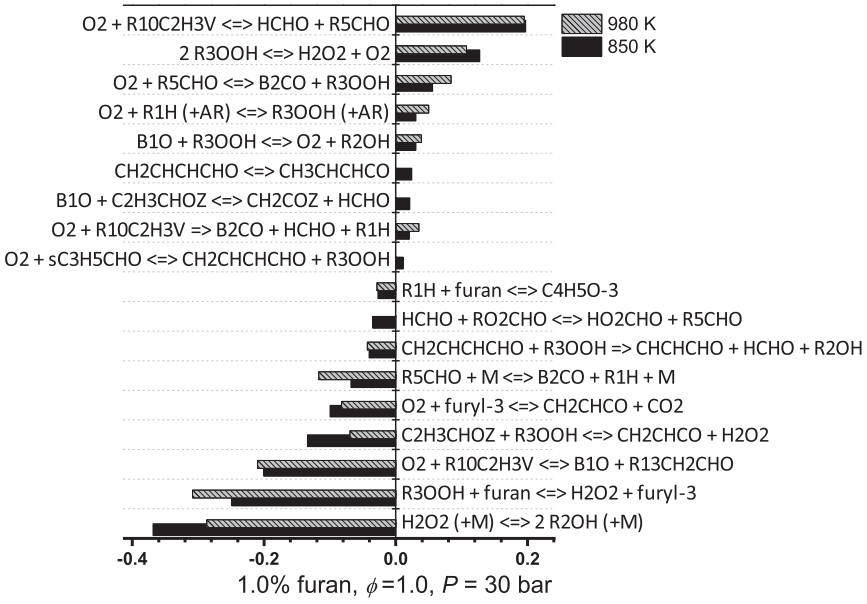

Fig. 6. Sensitivity analysis of furan ignition at 850 and 980 K using Tran mechanism [5].

3.4. Mechanism analysis and optimization

This section firstly focuses on the analyses of furan sub-model. Details of furan reaction pathways are compared between different mechanisms. Secondly, since the literature mechanisms can only predict well the oxidation of one of the three fuels studied in this work, an optimized model is proposed combining all the three fuel sub-mechanisms from literatures. Finally, the present mechanism is validated against the IDTs from RCM and shock tube [19,31], and species profiles from JSR [30].

3.4.1. Comparison of the furan sub-models

In order to investigate the differences existing among these mechanisms, reaction pathway analysis was conducted for stoichiometric furan at 18 bar and 900 K using the mechanism of Somers et al. [21,22] and Tran et al. [5], as shown in Fig. 4. Concerning primary consuming routes from the Somers mechanism, furan is mainly consumed (63.8%) by OH-addition reactions at C2 position, followed by H-addition reactions at C2. Being largely different from DMF25, MF2, and EF2, H-abstraction reactions (mainly by O and OH radicals) from C2 and C3 position only consumes 7.1% fuel due to the bond dissociation energy (BDE) differences in ring and allylic C–H bonds [32]. The differences in the relative importance of H-abstractions for furan and other alkylated furans also explain their different dependence on equivalence ratio. For alkylated furans, the fuel radicals resulted from H-abstractions mainly react with HO_2, CH_3O_2, and O_2 whose concentration is relevant with equivalence ratio. As to the mechanism of Tran et al. [5], the primary fuel consumption routes do 'not vary much. The OH-additions and H-additions account for more fuel consumption,

while that of H-abstractions decreases. H-abstraction by HO_2 account for 1.9% fuel consumption, and the generated H_2O_2 molecule would mainly decompose into 2 OH radicals in the low to intermediate temperature range. Being different from the Somers mechanism where OH-addition reaction of furan at C2, reactions of f2j and f3j with O_2 are one-step lumped reactions, the mechanism of Tran et al. [5] incorporated some new features in the furan submechanism. (1) Detailed OH-addition and subsequent isomerization and decomposition are included. Mousavipour et al. [33] studied the reactions of OH radical with furan and pointed out that substitution and H-abstractions by OH radicals are of significant importance above 2000 K, while OH-additions dominate at low temperatures, which is in accordance with the reaction pathways. Tran et al. [5] adopted the rate constant of the OH-addition reaction from the quantum chemistry calculation of Mousavipour et al. [33]; (2) The authors [5] updated the rate constants for H-abstraction reactions of the fuel with H, CH_3, and HO_2 radials as well. (3) The major pathways of radicals f2j and f3j are through disproportionation reactions; CH_2CHCO, the major product of f2j and f3j radicals, will not add H radical and generate CH_3CHCO which consumes OH radicals subsequently. Instead, CH_2CHCO decomposes into C_2H_3 and CO; (4) Tran et al. [5] newly introduced the reactions of radicals f2j, f3j, C_4H_5O-2, and C_4H_5O-3 with HO_2 and CH_3O_2 into the sub-mechanism. (5) The product of H-addition would disproportionate with HO_2 generating OH radicals.

Compared with Somers mechanism, Tran mechanism greatly enhances the simulated furan reactivity. This is mainly caused by two reasons: (1) the updated H-abstraction reactions with HO_2 radical, which would generate 2 OH radicals; (2) the decomposition reaction of CH_2CHCO prevent the subsequent OH consuming reactions.

In the low pressure oxidation study of Tran et al. [5], furan is mainly consumed through H-additions and OH-additions. One main feature distinguishes alkylfurans low temperature oxidation from that of alkylbenzenes is the large contribution of OH-addition to the fuel consumption. OH-addition at C5 position (no alkyl substitution site) of furan, MF and EF will generate C_2H_3CHO+ HCO, C_2H_3CHO+CH_3CO, and C_2H_3CHO+CH_3CH_2CO, respectively, while OH-addition at C2 position would yield C_2H_3CHO + HCO, methyl vinyl ketone + HCO, and ethyl vinyl ketone + HCO, respectively. Due to the symmetry of furan, OH-additions would produce equal amount of HCO radical, making its chemistry vital. Tran et al. [5] set the rate constant for reaction: HCO + O_2 = CO + HO_2 to 1/3 of its original value [34]. The influence of this reaction on IDTs is depicted in Fig. 5. Decreasing the rate constant of the reaction prevents the mechanism from correctly capture the trend of IDTs with equivalence ratio, while increasing the rate constant of this reaction strengthens the influence of equivalence ratio on IDTs.

Sensitivity analysis was conducted using Tran mechanism [5], as shown in Fig. 6. The IDTs of furan are very sensitive to the H-abstractions with HO_2 radical and vinyl radical oxidation. The rate constant of reaction: furan+R3OOH = furyl-3 + H_2O_2 in the mechanism of Tran et al. [5], which is from RMG [35], is about 2–8 magnitude higher than that in Somers mechanism [21,22] in the low to intermediate temperature range. The rate constant of this reaction along with others of similar H-abstraction by HO_2 reactions are compared in Fig. 7. Cyclopentane [38], a saturated five-member ring, has the highest rate constant. While, for H-abstraction in the C2 position of 1,3-butadiene [39], its rate constant is the lowest among the comparison due to the high C–H BDE. The C–H BDE is also very high for furan, yet the rate constant used in Tran mechanism [5] is even slightly higher than that of C_3H_8 and C_3H_6_allylic H-abstraction reactions calculated by Tsang [36,37] in the studied temperature range. Considering the large uncertainty of the important reactions, further mechanism development should put effort into the precise determination on the rate constants for H addition and H-abstraction by HO_2 radicals by using high-level quantum chemistry calculation. Moreover, for the unimolecular reactions: furan = $CH_2CCHCHO$ and furan = C_2H_2 + CH_2CO which accounts for most fuel consumption at the 20% fuel consumption, pressure dependent rate constants are also suggested.

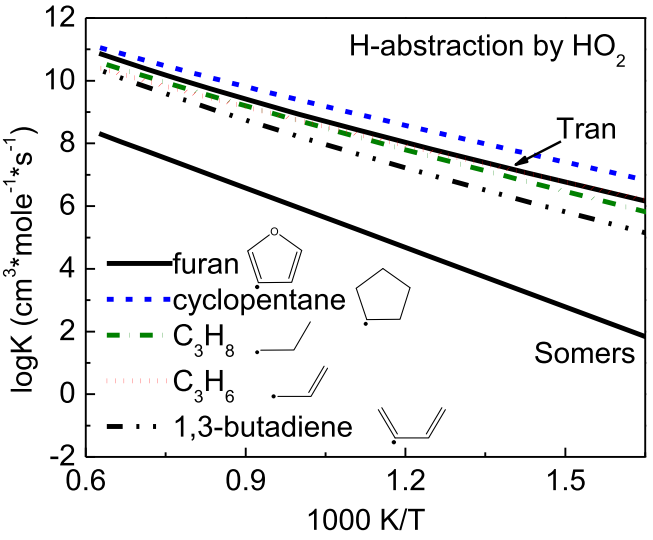

Fig. 7. Comparison on the rate constants of H-abstraction reactions. Furan (black lines): from Tran et al. [5] and Somers et al. [21,22]; cyclopentane (blue dash line): from Handford et al. [38]; C_3H_8 and C_3H_6 (green dash dot line and red dot line): from Tsang et al. [36,37]; 1,3-butadiene (black dash dot line): from AramcoMech 3.0 [39]. (For interpretation of the references to color in this figure legend, the reader is referred to the web version of this article.)

3.4.2. Low-temperature oxidation of THF

Reaction flux analysis of stochiometric THF mixture was conducted at 18 bar and 700 K, as shown in Fig. 8. The oxidation of THF has exhibited typical low-temperature reaction pathways: The tetrahydrofuran firstly goes through H-abstraction reactions by OH or HO_2 and gives tetrahydrofuranyl radicals. Tetrahydrofuranyl radicals then mainly add O_2 and produce ROO radicals, followed by internal isomerization and yield QOOH radicals. These QOOH radicals can either undergo ring opening by beta-scission and produce butanedial and OH, or second O_2 addition which subsequently go through HO_2 elimination and decompose into acrolein, HCO and OH radicals. Tetrahydrofuranyl radical (cy(OCJCCC)) can also directly go through ring opening (25.1%) and yield butanal-4-yl radical (C3H6CHO-1). The subsequent reactions of O_2 addition to C3H6CHO-1 are also included in the system which contributes to the low-temperature reactivity of THF oxidation.

Instead of O_2 addition, 23.8% tetrahydrofuranyl radicals form 2,3-dihydrofuran by concerted elimination of HO_2 radicals. 2,3-dihydrofuran reacts with OH by H-abstraction and give dihydrofuranyl radicals (C4H5O-2 and C4H5O-3). By analogy with tetrahydrofuranyl radicals, dihydrofuranyl radicals would also add O_2 and form ROO radicals, which finally eliminate an OH radical and decompose to acrolein and HCO radical. However, all the dihydrofuranyl radicals are ended up in forming furan while the O_2 addition and subsequent reactions are missing in the current mechanism of Fenard et al. [18], which could be the reason that Fenard mechanism is under-predicted the low-temperature reactivity of 2,3-DHF.

3.4.3. Mechanism optimization and validation

The recently developed mechanism of Fenard et al. [18] is based on a well-validated high-temperature model of Tran et al. [17] by adopting high-level theoretical calculations for important reactions. This model has shown quite good performance in predicting IDTs and oxidation species profiles of THF/oxygen mixtures.

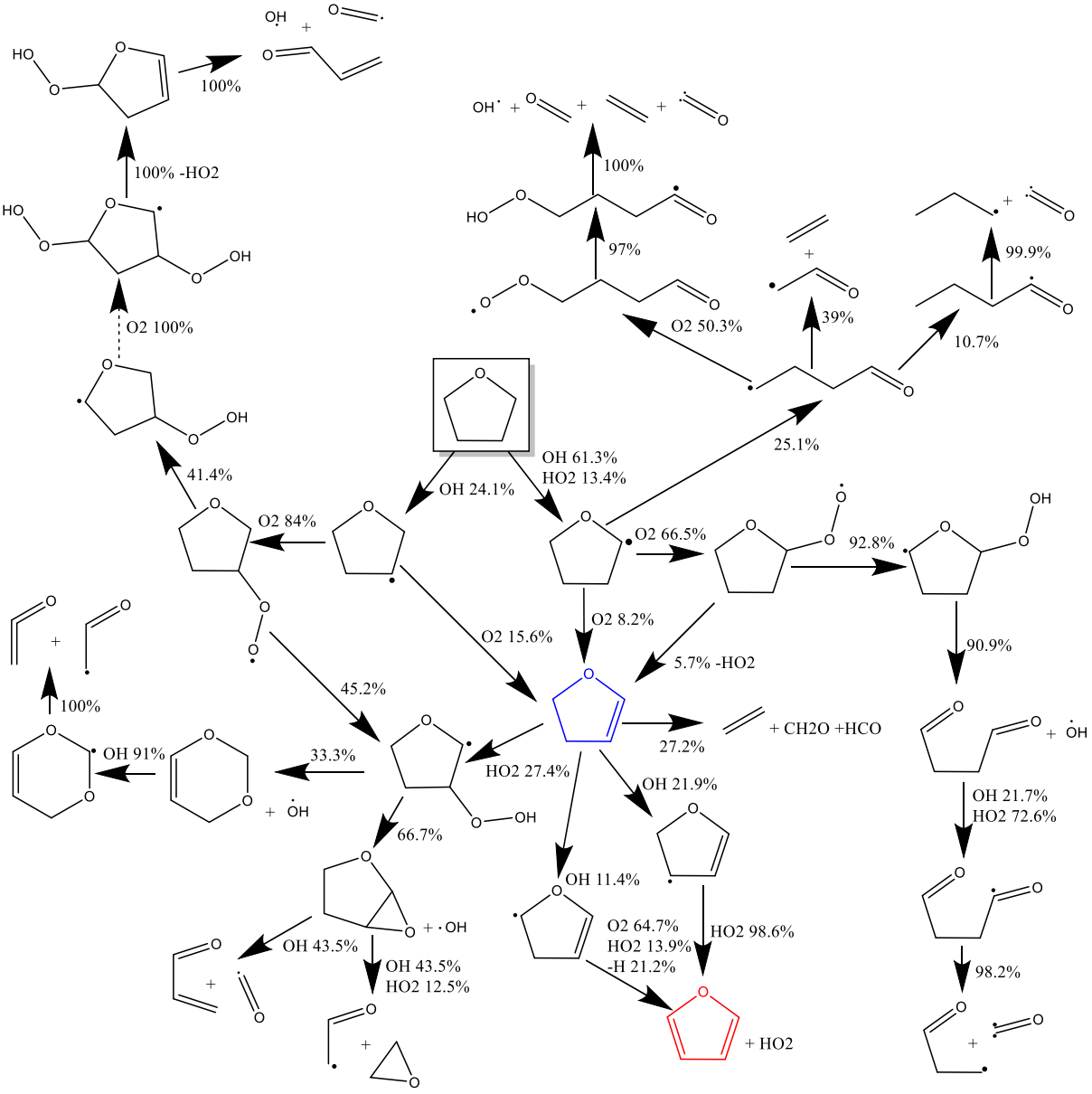

Fig. 8. Reaction flux analysis of 1% THF, $\phi = 1.0$, at 700 K, $p = 18$ bar, using Fenard model [18].

However, this model does not contain the newest features of low-temperature furan reactions and therefore cannot predict its ignition in a reasonable level. Considering the good performance of Fenard model [18] in predicting species profiles of C1–C4 hydrocarbons, acyclic and cyclic oxygenated compounds, we then employed the new features of furan sub-model from Tran mechanism [5]. 2,3-DHF sub-model was also modified by completing the reaction pathways and updating the rate constants for important reactions. Details of the mechanism optimization along with the present mechanism are provided in the supplementary materials.

Mechanism optimization: For the furan sub-mechanism, the rate constants of H-abstraction reactions are firstly updated to those in Tran mechanism [5]. The rate constant of H-abstraction from C3 position of furan by HO_2 is decreased by analogy with 1,3-butadiene, as discussed in Section 3.3.1. H abstracted by CH_3O_2, CH_2, and HCO which were missing in the original model are now added in the present model. Ring opening reactions are also included in the present model, especially for OH addition to furan generating HCOCHCHCHOH radical, which is found largely contributing to the consumption of furan in the studied low-to-intermediate temperature range [33]. Two new species (HCOCHCHCHOH, HCOCH2CHCHO) together with relevant reactions from Tran mechanism [5] are imported in the present mechanism to make sure they can be reacted with other species.

For 2,3-DHF sub-mechanism, firstly, H-abstraction reactions by HO_2, OH, HCO, CH_2OH, CH_3O, and C_2H_5 radicals are added or updated by analogy with THF in Fenard mechanism [18], and decreased Ea is adopted for H-abstraction reactions from allylic sites. Ring opening and decomposition reactions are important reactions in the consumption of furan [5] and THF [18], and thus these reactions of 2,3-DHF suggested by Fan et al. [19] are employed in the present model. However, integrating the above reactions only limitedly increased the reactivity of 2,3-DHF at low temperatures because dihydrofuranyl radicals have no other reaction pathways but all end up forming furan by eliminating another H atom, as shown in Fig. 8. Since detailed kinetic model development of

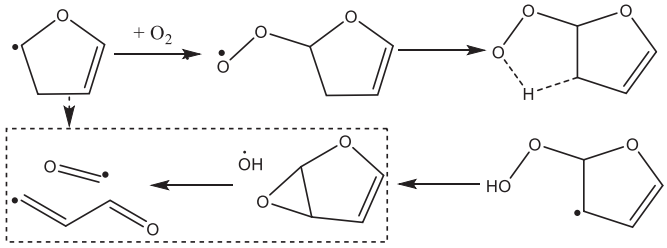

Fig. 9. The reaction pathways of O_2 addition to dihydrofuranyl radical.

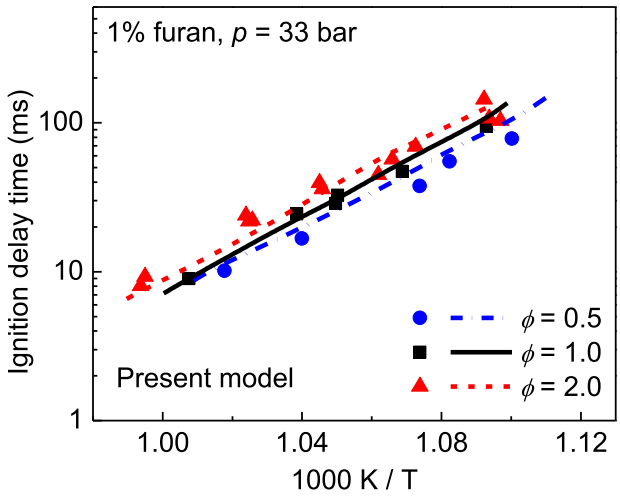

Fig. 10. The prediction of IDTs of furan under different equivalence ratios using the present model.

2,3-DHF is out of the scope of present work, and there are no thermal and kinetic data of O_2 addition and ring opening reactions in the literature, one-step lumped reactions of dihydrofuranyl radicals react with O_2, as shown in Fig. 9, are adopted in the present 2,3-DHF sub-mechanism. Adding these reactions greatly promotes the reactivities at temperatures lower than 1050 K, while the predictions at higher temperatures are little affected. It should be noted that, the rate constant of this reaction is just fitted to make better agreement with the experimental data and further quantum chemistry calculations are needed to precisely determine the intermediate products and rate constant of each step.

Mechanism validation: The present mechanism is firstly validated against IDTs of furan, 2,3-DHF and THF measured in this study. Furthermore, literature high temperature IDTs of furan [9], 2,3-DHF [19], and THF [31] in shock tube and JSR species profiles [30] are also simulated to evaluate the performance of the present mechanism. Compared with the literature model, present model generally shows improved predictions for furan, 2,3-DHF and THF oxidation.

Figure 10 shows the prediction of the IDTs of furan under ϕ = 0.5, 1.0 and 2.0, 33 bar conditions. Compared with the predictions of Tran model, as shown in Fig. 2(a), the effect of equivalence ratio is better captured in the present model. This improvement is mainly contributed by the updated base mechanism [18], especially reaction HCO + O_2 = CO + HO_2, which has adopted the original rate constant calculated by Timonen et al. [34].

Comparisons on the IDT predictions of furan at different pressures using Tran [5] and present models are shown in Fig. 11. Generally, these two models generate very similar performance, and present model has slightly improved the agreement between model predictions and experimental data.

Model predictions for the IDTs of 2,3-DHF and THF are shown in Fig. 12. The present model has shown a significant improvement

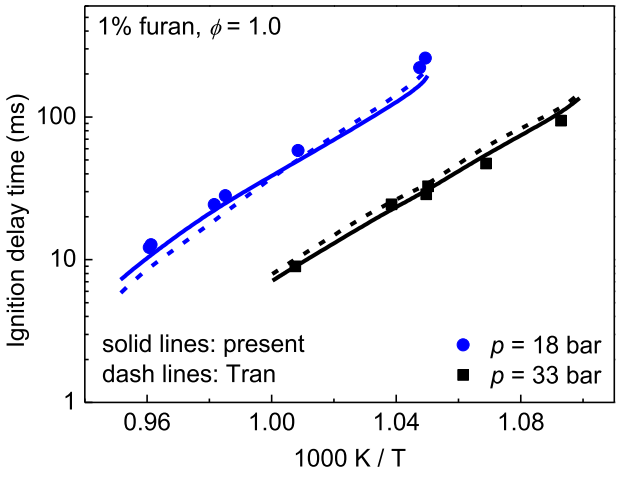

Fig. 11. Comparison on the simulated IDTs of furan at different pressures using Tran model [5] and present model.

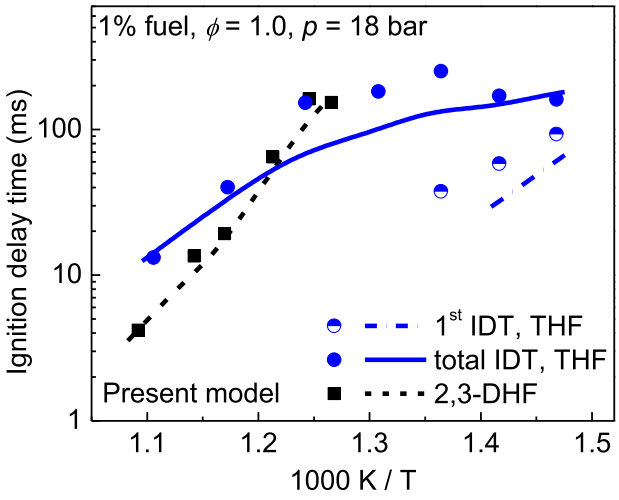

Fig. 12. Predicted IDTs of 2,3-DHF and THF using present model.

on the reactivity predictions and well captured the IDTs of 2,3-DHF. For the auto-ignition of THF, the present model yields similar performance as that of Fenard et al. [18].

Since the reactions in furan sub-mechanism are also important in high-temperature range, IDTs measured in a shock tube by Wei et al. [9] are also simulated using present model. Figure 13 shows that present model can also better predict the auto-ignition of furan up to 1900 K, under various pressure and equivalence ratio conditions.

Figure 14 presents performance assessment of the present model concerning IDTs of 2,3-DHF measured by Fan et al. [19] and THF measured by Uygun et al. [31] in shock tubes. Compared with Fenard model [18], the present model shows a significant improvement in predicting the IDTs of 2,3DHF and slight improved performance for autoignition of THF.

The mole fraction profiles of furan, 2,3-DHF and THF obtained in a JSR by Vanhove et al. [30] are simulated at equivalence ratio 0.5, 1.0 and 2.0, as shown in Fig. 15. The present model shows a same prediction with Fenard model [18] in the profiles of THF under different equivalence ratio. While for furan and 2,3-DHF, predictions of the present model are getting closer to the experimental data. The present model also reproduces the product mole fractions well such as CH_2O and CO_2 etc. which are provided in the supplementary material along with further validations against IDTs in the literatures.

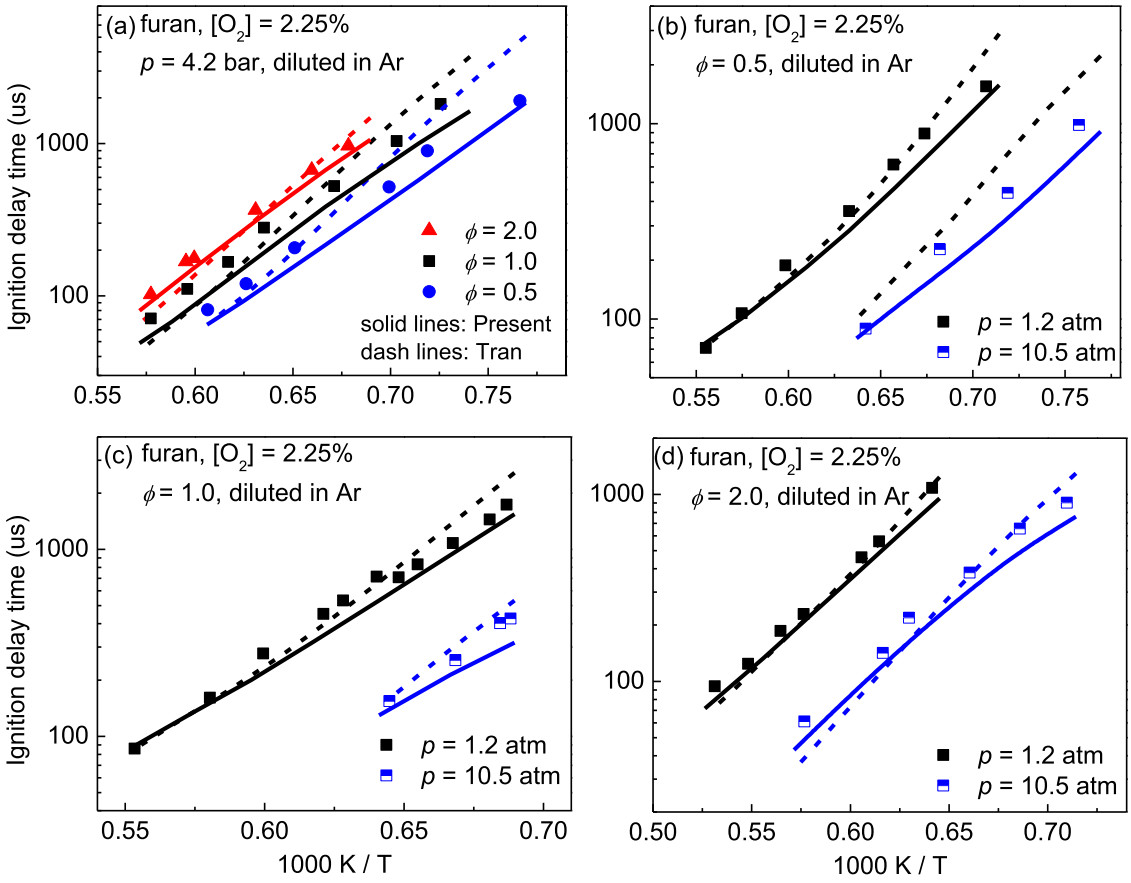

Fig. 13. Comparison on the simulated IDTs of furan from shock tube measurement by Wei et al. [9] using Tran model [5] and present model.

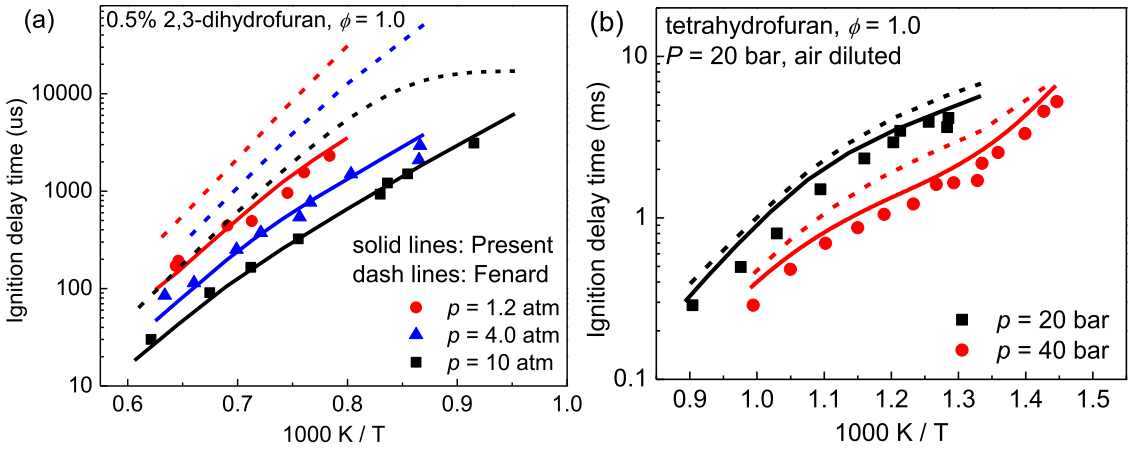

Fig. 14. Comparison on the simulated IDTs of 2,3-DHF(a) from Fan et al. [19] and THF (b) from Uygun et al. [31] using Fenard model [18] and present model.

3.5. Discussion on furan: the starting point of furan derivatives

Furan is a base molecule for investigating furan derivatives: by adding alkyl side chains generates alkylfurans; by increasing the saturation extent generates dihydrofurans and tetrahydrofuran. Figure 16 shows the comparison on IDTs of furan, alkylfurans [6], 2,3-DHF, and THF in the low to intermediate temperatures under 1% fuel concentration, stoichiometric conditions, and pressures of 16–18 bar. It can be seen from Fig. 16 that the reactivity of furan is the lowest among alkylfurans, 2, 3-dihydrofuran and tetrahydrofuran. Our previous work pointed out that H-abstractions at alkyl site contribute 1/3 of alkylfuran fuel consumption [6,29], and recombination/disproportionation reactions between fuel and HO_2 radicals greatly enhance the reactivity. Due to the unsaturated nature of furan ring, the reaction pathway of furan differs: OH-additions and H-additions dominate, while H-abstraction becomes a minor route.

Another interesting comparison is among furan, 2,3-DHF, and THF, illustrating the influence of the double bond number on the low temperature reactivity. It can be seen from furan to THF, increasing the saturation degree greatly improves combustion reactivity, especially at lower temperatures. The IDTs of furan are more than one magnitude higher than those of 2,3-DHF and THF. The reactivity of 2,3-DHF is slightly higher than THF in the higher temperature range (>810 K) while THF exhibits higher reactivity and NTC behavior below 730 K. From THF to furan, inducing more double bonds on the ring has greatly changed the ring C–H bond

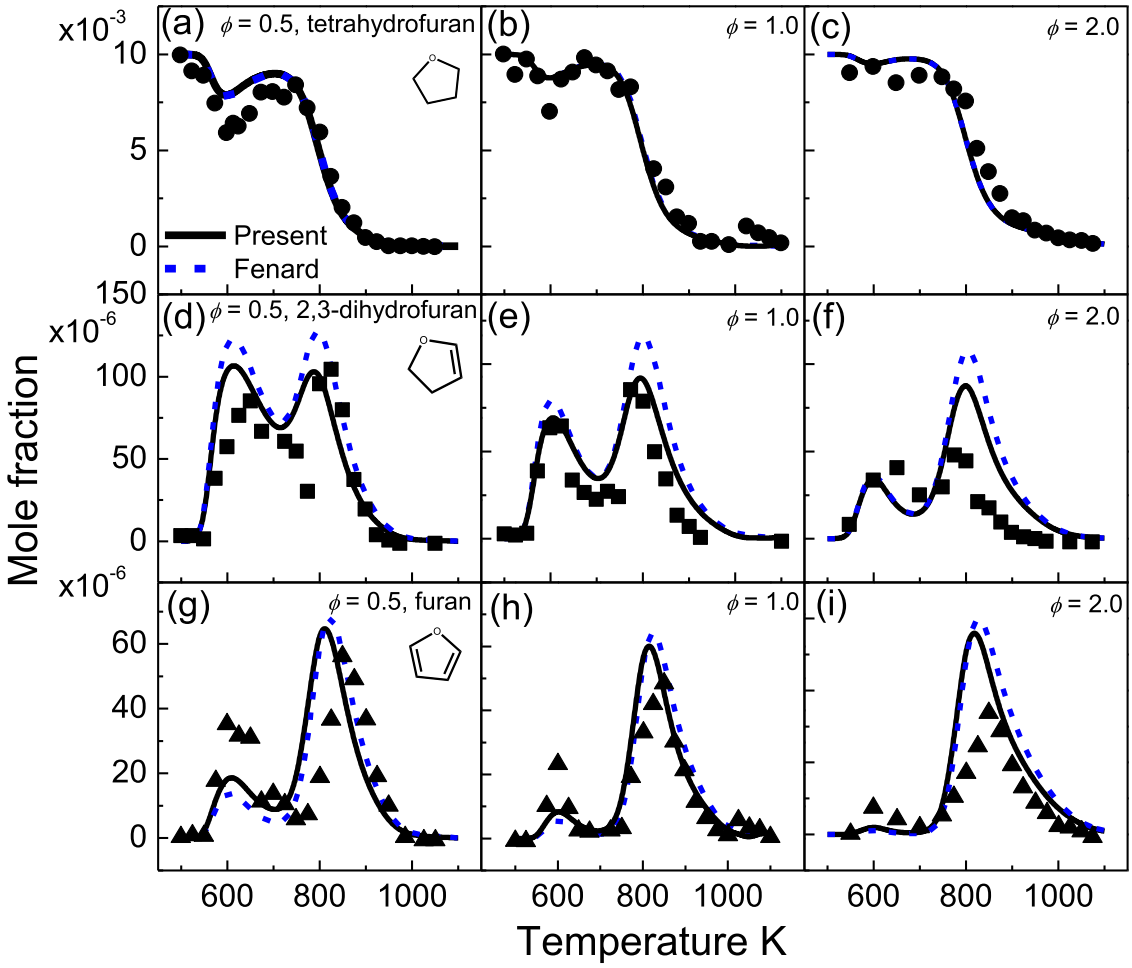

Fig. 15. Comparison on the simulated mole fraction profiles for THF, 2,3-DHF and furan under different equivalence ratios in a JSR from Vanhove et al. [30], solid lines: present model; dash lines: Fenard model [18].

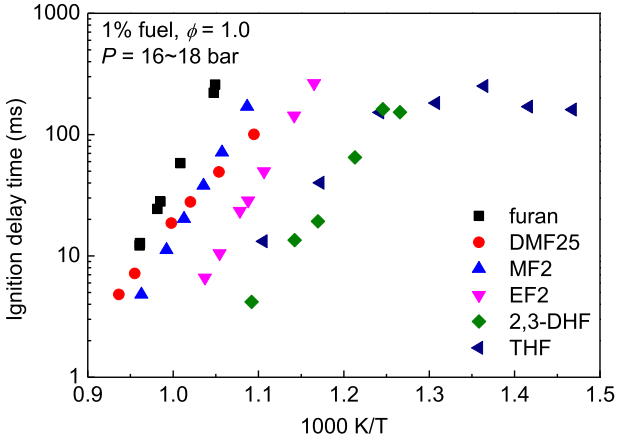

Fig. 16. Comparison on IDTs of furan, 2,3-DHF, THF and alkylfurans at 16–18 bar, 1% fuel concentration, and ϕ = 1.0. Black squares: furan; red circles: DMF25; blue triangles [29]: MF2; violet triangles [29]: EF2; green diamonds [6]: 2,3-DHF; purple triangles: THF. (For interpretation of the references to color in this figure legend, the reader is referred to the web version of this article.)

dissociation energies [16]. For THF, the C3-H BDE is 411.6 kJ/mol, and that of C2–H is ~20 kJ/mol lower as it is more adjacent to the O atom. The C3–H BDE (allylic) in 2,3-DHF is only 343.8 kJ/mol, which is 48.6 kJ/mol lower than that of C2–H in THF, making it easier to be broken. Furan has two functional groups: O atom and two double bonds. However, the double bonds on furan molecule are not discrete because of its aromatic system like benzene, and the ring C–H BDE is around 504 kJ/mol, no matter at C2 or C3. The low temperature reactivity largely depends on the two sequences of O_2 addition, internal H-shift and isomerization, which generates two OH radicals. For furan, this sequence is not favored at low temperature due to the BDE and number of C–H on the ring. Comparing with alkyl side chains (1 or 2 C atoms) substitution, saturation degree of furan derivatives has a more notably influence on low to intermediate temperature reactivity enhancement. Without the dominating effect of ring double bonds, the presence of O atom lowers the ring C–H BDEs of THF and saturated part of 2,3-DHF, making them lower than the methyl C–H BDE. Besides, removing one double bond also increase the number of available adjacent H atoms, facilitating the two internal H-abstractions involved in the low to intermediate temperature chain branching sequence.

4. Conclusions

The present work measured the low to intermediate temperature IDTs of furan at 1% fuel concentration, 18 and 33 bar, and equivalence ratios of 0.5, 1.0, and 2.0. The IDTs of furan lengthen with the decreasing pressure and are not sensitive to equivalence ratio variation. Comparation among furan, alkylated furans, 2,3-DHF, and THF indicates that saturation degree has a more dominant effect on enhancing the low to intermediate temperature reactivity compared with alkyl substitution.

The literature mechanisms were validated against present data. Kinetic analyses were conducted to reveal the major consuming pathways of furan and the causes for the deviation between mechanism prediction and experimental data. In the low to intermediate temperature range, furan is mainly consumed by OH-addition and H-addition reactions, while H-abstraction only account for a minor part. Uncertainty remains in the rate constant of reaction: furan + R3OOH = furyl-3 + H_2O_2 which greatly promotes reactivity.

A kinetic mechanism has been optimized including the submodels of furan, 2,3-DHF and THF, and it shows improved performance in predicting the IDTs as well as products mole fraction profiles in a JSR.

Declaration of Competing Interest

The authors declare that they have no known competing financial interests or personal relationships that could have appeared to influence the work reported in this paper.

Acknowledgment

This work is supported by the National Natural Science Foundation of China (51722603) and the Fundamental Research Funds for the Central Universities. CT is a Tang Scholar and he appreciates the support from by Open Research Fund of Beijing Key Laboratory of Powertrain for New Energy Vehicle, Beijing Jiaotong University. YW would like to thank the support from the China Scholarship Councial (NO. 201806280105).

Supplementary materials

Supplementary material associated with this article can be found, in the online version, at doi:10.1016/j.combustflame.2019.12.010.

References

[1] M.R. Grochowski, W. Yang, A. Sen, Mechanistic study of a one-step catalytic conversion of fructose to 2,5-dimethyltetrahydrofuran, Chem. Eur. J. 18 (39) (2012) 12363–12371.
[2] J.-P. Lange, E. van der Heide, J. van Buijtenen, R. Price, Furfural—a promising platform for lignocellulosic biofuels, ChemSusChem 5 (1) (2012) 150–166.
[3] L.W. Burnett, I.B. Johns, R.F. Holdren, R.M. Hixon, Production of 2-methylfuran by vapor-phase hydrogenation of furfural, Ind. Eng. Chem. 40 (3) (1948) 502–505.
[4] W.S. Schlotzhauer, R.F. Arrendale, O.T. Chortyk, The rapid pyrolytic characterization of tobacco leaf carbohydrate material, J. BTFI GmbH 13 (2) (1985) 74–80.
[5] L.-S. Tran, Z. Wang, H.-H. Carstensen, C. Hemken, F. Battin-Leclerc, K. Kohse-Höinghaus, Comparative experimental and modeling study of the low-to moderate-temperature oxidation chemistry of 2, 5-dimethylfuran, 2-methylfuran, and furan, Combust. Flame 181 (2017) 251–269.
[6] N. Xu, Y. Wu, C. Tang, P. Zhang, X. He, Z. Wang, et al., Ignition delay times of low alkylfurans at high pressures using a rapid compression machine, Proc. Combust. Inst. 36 (1) (2017) 323–332.
[7] A.M. Eldeeb, B. Akih-Kumgeh, Recent trends in the production, combustion and modeling of furan-based fuels, Energies 11 (3) (2018) 512.
[8] Z. Tian, T. Yuan, R. Fournet, P.A. Glaude, B. Sirjean, F. Battin-Leclerc, et al., An experimental and kinetic investigation of premixed furan/oxygen/argon flames, Combust. Flame 158 (4) (2011) 756–773.
[9] L. Wei, C. Tang, X. Man, X. Jiang, Z. Huang, High-temperature ignition delay times and kinetic study of furan, Energy Fuels 26 (4) (2012) 2075–2081.
[10] D. Liu, C. Togbe, L.S. Tran, D. Felsmann, P. Osswald, P. Nau, et al., Combustion chemistry and flame structure of furan group biofuels using molecular-beam mass spectrometry and gas chromatography – Part I: furan, Combust. Flame 161 (3) (2014) 748–765.
[11] L.S. Tran, C. Togbe, D. Liu, D. Felsmann, P. Osswald, P.A. Glaude, et al., Combustion chemistry and flame structure of furan group biofuels using molecular-beam mass spectrometry and gas chromatography – Part II: 2-methylfuran, Combust. Flame 161 (3) (2014) 766–779.
[12] C. Togbe, L.S. Tran, D. Liu, D. Felsmann, P. Osswald, P.A. Glaude, et al., Combustion chemistry and flame structure of furan group biofuels using molecular-beam mass spectrometry and gas chromatography – Part III: 2,5-dimethylfuran, Combust. Flame 161 (3) (2014) 780–797.
[13] M.A. Eldeeb, B. Akih-Kumgeh, Reactivity trends in furan and alkyl furan combustion, Energy Fuels 28 (10) (2014) 6618–6626.
[14] N. Xu, C. Tang, X. Meng, X. Fan, Z. Tian, Z. Huang, Experimental and kinetic study on the ignition delay times of 2, 5-dimethylfuran and the comparison to 2-methylfuran and furan, Energy Fuels 29 (8) (2015) 5372–5381.
[15] A. Sudholt, L. Cai, J. Heyne, F.M. Haas, H. Pitsch, F.L. Dryer, Ignition characteristics of a bio-derived class of saturated and unsaturated furans for engine applications, Proc. Combust. Inst. 35 (3) (2015) 2957–2965.
[16] A. Sudholt, C. Lee, J. Klankermayer, R.X. Fernandes, H. Pitsch, Ignition characteristics of saturated and unsaturated furans, Combust. Flame 171 (2016) 133–136.
[17] L.-S. Tran, M. Verdicchio, F. Monge, R.C. Martin, R. Bounaceeur, B. Sirjean, et al., An experimental and modeling study of the combustion of tetrahydrofuran, Combust. Flame 162 (5) (2015) 1899–1918.
[18] Y. Fenard, A. Gil, G. Vanhove, H.-H. Carstensen, K.M. Van Geem, P.R. Westmoreland, et al., A model of tetrahydrofuran low-temperature oxidation based on theoretically calculated rate constants, Combust. Flame 191 (2018) 252–269.
[19] X. Fan, X. Wang, J. Wang, K. Yang, Comparative shock tube and kinetic study on high-temperature ignition of 2,3-dihydrofuran and 2,5-dihydrofuran, Energy Fuels 30 (10) (2016) 8727–8736.
[20] X.S. Fan, X.B. Wang, K.K. Yang, Y.T. Li, C.Z. Wu, Z.Q. Li, Experimental and modeling study on ignition characteristics of 2, 5-dihydrofuran, SAE Int. J. Fuels Lubr. 9 (1) (2016) 315–321.
[21] K.P. Somers, J.M. Simmie, F. Gillespie, C. Conroy, G. Black, W.K. Metcalfe, et al., A comprehensive experimental and detailed chemical kinetic modelling study of 2,5-dimethylfuran pyrolysis and oxidation, Combust. Flame 160 (11) (2013) 2291–2318.
[22] K.P. Somers, J.M. Simmie, W.K. Metcalfe, H.J. Curran, The pyrolysis of 2-methylfuran: a quantum chemical, statistical rate theory and kinetic modelling study, Phys. Chem. Chem. Phys. 16 (11) (2014) 5349–5367.
[23] H. Di, X. He, P. Zhang, Z. Wang, M.S. Wooldridge, C.K. Law, et al., Effects of buffer gas composition on low temperature ignition of iso-octane and n-heptane, Combust. Flame 161 (10) (2014) 2531–2538.
[24] Y. Wu, M. Yang, C. Tang, Y. Liu, P. Zhang, Z. Huang, Promoting “adiabatic core” approximation in a rapid compression machine by an optimized creviced piston design, Fuel 251 (2019) 328–340.
[25] Y. Liu, C. Tang, C. Zhan, Y. Wu, M. Yang, Z. Huang, Low temperature auto-ignition characteristics of methylcyclohexane/ethanol blend fuels: ignition delay time measurement and kinetic analysis, Energy 177 (2019) 465–475.
[26] M. Yang, Y. Wu, C. Tang, Y. Liu, Z. Huang, Auto-ignition behaviors of nitromethane in diluted oxygen in a rapid compression machine: critical conditions for ignition, ignition delay times measurements, and kinetic modeling interpretation, J. Hazard Mater. 377 (2019) 52–61.
[27] C.-J. Sung, H.J. Curran, Using rapid compression machines for chemical kinetics studies, Prog. Energy Combust. Sci. 44 (2014) 1–18.
[28] ANSYS Chemkin-Pro® Academic Research, Release 18.2. ANSYS Inc.
[29] N. Xu, Y. Wu, C. Tang, P. Zhang, X. He, Z. Wang, et al., Experimental study of 2,5-dimethylfuran and 2-methylfuran in a rapid compression machine: comparison of the ignition delay times and reactivity at low to intermediate temperature, Combust. Flame 168 (2016) 216–227.
[30] G. Vanhove, Y. Yu, M.A. Boumehdi, O. Frottier, O. Herbinet, P.-A. Glaude, et al., Experimental study of tetrahydrofuran oxidation and ignition in low-temperature conditions, Energy Fuels 29 (9) (2015) 6118–6125.
[31] Y. Uygun, S. Ishihara, H. Olivier, A high pressure ignition delay time study of 2-methylfuran and tetrahydrofuran in shock tubes, Combust. Flame 161 (10) (2014) 2519–2530.
[32] A. Sudholt, L. Cai, J. Heyne, F.M. Haas, H. Pitsch, F.L. Dryer, Ignition characteristics of a bio-derived class of saturated and unsaturated furans for engine applications, Proc. Combust. Inst. 35 (3) (2014) 2957–2965.
[33] S.H. Mousavipour, S. Ramazani, Z. Shahkolahi, Multichannel RRKM-TST and direct-dynamics VTST study of the reaction of hydroxyl radical with furan, J. Phys. Chem. A 113 (12) (2009) 2838–2846.
[34] R.S. Timonen, E. Ratajczak, D. Gutman, Kinetics of the reactions of the formyl radical with oxygen, nitrogen dioxide, chlorine, and bromine, J. Phys. Chem. 92 (3) (1988) 651–655.
[35] C.W. Gao, J.W. Allen, W.H. Green, R.H. West, Reaction mechanism generator: automatic construction of chemical kinetic mechanisms, Comput. Phys. Commun. 203 (2016) 212–225.
[36] W. Tsang, Chemical kinetic data base for combustion chemistry. Part 3: propane, J. Phys. Chem. Ref. Data 17 (2) (1988) 887–951.
[37] W. Tsang, Chemical kinetic data base for combustion chemistry. Part V: propene, J. Phys. Chem. Ref. Data 20 (2) (1991) 221–273.
[38] S.M. Handford-Styring, R.W. Walker, Rate constants for the reaction of HO_2 radicals with cyclopentane and propane between 673 and 783 K, Phys. Chem. Chem. Phys. 4 (4) (2002) 620–627.
[39] C.-W. Zhou, Y. Li, U. Burke, C. Banyon, K.P. Somers, S. Ding, et al., An experimental and chemical kinetic modeling study of 1,3-butadiene combustion: ignition delay time and laminar flame speed measurements, Combust. Flame 197 (2018) 423–438.